Helsinki University of Technology
Faculty of Electronics, Communications and Automation
Department of Electrical Engineering

Determination of coefficients of thermal convection in a high-speed electrical machine

Mikko Jääskeläinen

Master's thesis submitted in partial fulfilment of the requirements for the degree of Master of Science in Technology

Espoo 31.08.2009

Supervisor: Prof. Antero Arkkio
Instructor: M.Sc Zlatko Kolondzovski

HELSINKI UNIVERSITY OF TECHNOLOGY Faculty of Electronics, Communications and Automation	ABSTRACT OF MASTER'S THESIS

Author	Mikko Jääskeläinen	Date	31.08.2009
		Pages	11 + 45
Title of thesis	Determination of coefficients of thermal convection in a high-speed electrical machine		
Professorship	Electromechanics	Code	S-17
Supervisor	Prof. Antero Arkkio		
Instructor	M.Sc Zlatko Kolondzovski		

Heat-transfer coefficients for a high-speed electrical machine are calculated in this work. The machine is divided in different subregions and the average heat-transfer coefficient for every region is calculated.

The heat-transfer coefficients are calculated analytically and numerically with a computer program. The analytical approach provides simple equations for calculating the heat-transfer coefficients. The analytical equations provide only the average value for the heat-transfer coefficients.

A computer program uses computational fluid dynamics for the numerical calculation. The program creates a finite element mesh from the 2-D model of the machine. After that, the temperature field, the velocity field and the pressure field are solved numerically. With the program, the inlet and the outlet values of the local heat-transfer coefficients are calculated.

The idea of the thesis is to compare the analytically calculated heat-transfer coefficients to the numerically calculated heat-transfer coefficients. Results are compared to each other and conclusions are made.

convection, heat transfer, high-speed machine, computational fluid dynamics

TEKNILLINEN KORKEAKOULU Elektroniikan, tietoliikenteen ja automaation tiedekunta		DIPLOMITYÖN TIIVISTELMÄ
Tekijä	Mikko Jääskeläinen	Päiväys 31.08.2009
		Sivumäärä 11 + 45
Työn nimi	Suurnopeuskoneen lämmönsiirtokertoimien määrittäminen	
Professuuri	Sähkömekaniikka	Koodi S-17
Työn valvoja	Prof. Antero Arkkio	
Työn ohjaaja	M.Sc Zlatko Kolondzovski	

Tässä työssä määritetään lämmönsiirtokertoimet suurnopeuskoneelle. Kone on jaettu eri osiin ja lämmönsiirtokerroin jokaiselle osalle määritetään.

Lämmönsiirtokerroin lasketaan analyyttisesti kaavoilla ja numeerisesti tietokoneohjelman avulla. Analyyttiset kaavat antavat yksinkertaiset yhtälöt lämmönsiirtokertoimen laskentaan ja ne antavat vain yhden arvon jokaiselle osalle.

Tietokoneohjelma käyttää laskentaan laskennallista virtaustekniikkaa. Ohjelma luo elementtiverkon koneen kaksiulotteisesta aksiaalimallista. Tämän jälkeen lämpötila-, nopeus- ja painekenttä voidaan ratkaista numereerisesti. Ohjelman avulla saadaan laskettua jokaisen osan sisäänmeno- ja ulostuloarvo lämmönsiirtokertoimelle.

Työn ajatuksena on vertailla laskettuja lämmönsiirtokertoimia simuloituihin lämmönsiirtokertoimiin. Tuloksia on vertailtu ja niistä on tehty johtopäätökset.

konvektio, lämmönsiirto, suurnopeuskone, laskennallinen virtaustekniikka

Preface

This master's thesis is done in the Department of Electrical Engineering in Helsinki University of Technology. The thesis is done in conjunction with the laboratory's work on thermal design of a high-speed permanent-magnet machine.

I want to thank my supervisor Professor Arkkio for providing me an opportunity to make my thesis in his group during this hard economic time.

I also want to thank my family for supporting me during my studies, both financially and mentally, and during my writing process of the thesis. Especially I want to thank my instructor Zlatko Kolondzovski for the instructions and patience he gave me during the writing process.

Espoo, 17.7.2009 Mikko Jääskeläinen

Contents

Symbols and Abbreviations

A_C	cross-section of a cooling channel, cross-section of a tube
A_s	surface area
B	dimensionless temperature gradient
C	constant
c	constant
$\mathrm{C}_{\epsilon 1}$	model constant
$\mathrm{C}_{\epsilon 2}$	model constant
C_f	local friction coefficient
C_m	torque coefficient
c_p	specific heat of the fluid, gas constant
c_v	specific heat at constant volume
C_μ	model constant
C_1	coefficient 1 for the Nusselt number of a cylinder, constant
C_2	coefficient 2 for the Nusselt number of a cylinder, constant
D	diameter of a cylinder, diameter of a tube
D_h	hydraulic diameter
d	diameter of a cylinder
d_h	characteristic length
E_t	thermal energy
$\mathbf{F}$	force vector
f	friction factor
F_g	geometrical factor
g	gravitational acceleration
Gr	Grashof number
h	local heat-transfer coefficient
$\bar{h}$	average heat-transfer coefficient
h_em	empirically calculated average heat-transfer coefficient
$\bar{h}_L$	average value of h for the entire tube
h_nu	numerically calculated average heat-transfer coefficient
k	constant
k_a	Karman's constant
k_eff	effective thermal conductivity
k_f	coefficient of thermal conductivity of the fluid
k_t	turbulent conductivity
k_w	turbulent kinematic energy

k_0	coefficient for the resistive losses in stator and rotor
k_1	coefficient for the hysteresis losses in the iron core
k_2	coefficient for eddy current losses in the conductors, iron core and frame
k_3	coefficient for friction losses
L	length of a tube, characteristic dimension of the body
l	length of the stator yoke, characteristic dimension of the geometry channel length
m	constant
m	mass of the fluid
n	coefficient for the Dittus-Boelter equation
n	rotation speed
Nu	Nusselt number
Nu_D	Nusselt number for a tube
$Nu_{D,\mathrm{fd}}$	Nusselt number for a fully developed region
$\mathbf{P}$	pressure vector
P	function describing the properties of a turbulent flow wetted perimeter, surface perimeter
P_{loss}	losses of a high-speed machine
P_{g}	coefficient for the geometrical factor
Pr	Prandtl number
Pr_{T}	turbulent Prandtl number
q	global heat flux, heat flux
q''	local heat flux
q_{conv}	total tube heat-transfer rate
q''_{s}	surface heat flux
r	radius of the rotor disk, radial coordinate
r_{m}	average of the stator and rotor radii
r_0	tube radius
Re	Reynolds number
Re_D	Reynolds number for a tube, Reynolds number for a cylinder
Re_{c}	critical Reynolds number
Re_{r}	tip Reynolds number
T	temperature
T_{m}	mean temperature of a tube
$T_{\mathrm{m,i}}$	mean temperature at the tube inlet
$T_{\mathrm{m,o}}$	mean temperature at the tube outlet
T_{w}	wall temperature
T^+	dimensionless wall distance
Ta	Taylor number
Ta_{m}	modified Taylor number
T_{s}	surface temperature
T_{o}	tube outlet temperature
T_{i}	tube inlet temperature
T_∞	free stream temperature of the fluid flow

$\mathbf{U}$	averaged velocity field vector
u	velocity component along a surface
u_m	mean velocity
u_τ	friction velocity
u_∞	free stream velocity
V	velocity of the fluid
v	velocity of the fluid
x	horizontal coordinate
x_c	critical distance
x_fd	entry length of a tube
$x_\mathrm{fd,h}$	hydrodynamic entry length
$x_\mathrm{fd,t}$	thermal entry length
y	vertical coordinate
y^+	wall distance
α	thermal diffusivity
β	model constant
δ	air-gap length
δ_T	thickness of the thermal boundary layer
δ_v	thickness of the velocity boundary layer
ϵ	dissipation rate of the turbulent energy
θ	angle
κ	turbulent kinetic energy
μ	dynamic viscosity of the fluid
μ_s	dynamic viscosity of the fluid at the surface temperature
μ_t	turbulent kinematic viscosity
ν	velocity component normal to a surface
ω	angular velocity
ρ	density of the fluid
σ_k	model constant
σ_e	model constant
τ_s	surface shear stress

Subscripts

0	initial value
conv	convection
fd,t	thermally fully developed
i	tube inlet
o	tube outlet
lam	laminar
m	mean value
s	surface

Other Notations

$f(x)$	function of x
$\dot{x}$	time derivative of x
x'	derivative of x
$\bar{x}$	mean value of x
Δx	difference $x_\infty - x_0$
$\frac{\partial}{\partial x}$	derivative with respect to x
$\mathbf{X}$	X-vector
$X(r, x)$	X as a function of r and x
X^T	transpose of a X-matrix

Abbreviations

CFD	computational fluid dynamics
PM	permanent magnet
rpm	rounds per minute

Chapter 1

Introduction

A high-speed electrical machine is an electrical machine intended to run typically between 20 000 rpm - 100 000 rpm. A high peripheral speed sets challenges to a rotor design. The rotor must be constructed as rigidly as possible.

Losses generated in a high-speed machine are comparable to those of a 50 Hz motor. But the size of the machine is smaller. Actually, the same amount of losses are generated in a smaller dimension. So the loss density in a high-speed machine is much higher. Because of this, a proper heat transfer is needed in a high-speed machine.

Heat is a form of energy that can be transferred from one system to another system. Heat transfer is a phenomenon in which heat is transferred from a hotter place to a colder place. The temperature difference is needed. Without it, there will not be any heat transfer. There are three kinds of heat-transfer mechanisms: conduction, convection and radiation.

Conduction can happen in solid, in liquid or in gas. Conduction happens due to collisions and diffusion of the molecules during their random motion. In solids, conduction happens due to the combination of vibrations of the molecules in a lattice and the energy transport by free electrons. The rate of a heat conduction is determined by a geometry of an object, a thickness of an object and a temperature difference across a medium.

Convection is a heat-transfer mode which happens between a solid surface and a liquid or gas, which is moving. The faster the fluid motion, the greater the heat-transfer effect. If the fluid is stationary, the heat transfer happens by free conduction. The convection is forced if the fluid is forced to flow over the surface by external means such as a fan, a pump or a wind. The free convection happens when the fluid motion is caused by density differences in the fluid. Usually density differences appear in the fluid because of temperature differences in the fluid.

Radiation is the last mode of the heat transfer. Radiation does not need the presence of a medium, like convection and conduction. Radiation happens due to electromagnetic waves as a result of the changes in the electromagnetic configurations of the atoms or molecules. In heat-transfer studies, we are interested in thermal radiation, which is of the form of radiation emitted by bodies because of their temperature. All objects above the absolute zero temperature transmit radiation to varying degrees. The maximum rate of radiation that can be emitted from the surface is given by the Stefan-Boltzmann law.

A study of heat transfer in electrical machines is important. There are certain things in electrical machines which needs to be concerned of. In permanent-magnet machines, the demagnetization of the magnets is one thing. Also the carbon-fibre sleeve, which holds the the magnets, is sensitive for the temperature. The insulation of the winding has a temperature limit which cannot be exceeded.

Convection is mainly the phenomenon which transfers heat out from the machine. Convection is the most effective way to cool the machine. Flows inside the machine are usually turbulent which increases the heat transfer inside the machine. The most important cooling channel for the machine is an air gap. The air-gap flow removes heat generated in the rotor. It also removes friction losses and part of the stator losses.

The computational fluid dynamics is the newest method to model the heat transfer in a high-speed machine. It is a numerical method which solves the pressure, the velocity and the temperature field simultaneously. With numerical methods, we can model accurately the convection heat-transfer phenomenon. More about the basics of the heat transfer can be found in the work of Çengel (2002).

Chapter 2

High-speed electrical machine

2.1 High-speed drive systems

There are two kinds of electric drive systems for high-speed applications. An electrical network is feeding the system with 50 Hz or with 60 Hz. A conventional system, described in Figure 2.1a, includes a gearbox which is added behind the electrical machine. The gearbox raises the rotational speed. Another and a newer system is to include a frequency converter between the network and the machine. The frequency converter changes the frequency of the current which is fed to the machine. This kind of system is called a high-speed electric drive and is described in Figure 2.1b.

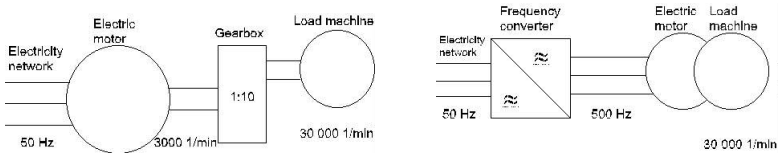

(a) *(b)*

Figure 2.1: Two different high-speed electrical systems.

2.2 Construction of high-speed electrical machines

Normally, high-speed electrical machines do not produce so much torque. That is why they are quite small machines. A stator winding is usually a normal three-phase winding. A high-frequency current is needed to supply the winding. Therefore, the stator winding is also typically a filamentary winding which is generally used in high-frequency transformers and inductors.

One important problem in high-speed machines are flux density harmonics. Flux density harmonics appear in the air gap because due to two reasons: A non-sinusoidal magnetic flux-density wave and a permeance difference in the air gap. There is a study of slot harmonics and winding harmonics in the work of Pyrhönen (1991). High-frequency flux harmonics affect the losses in the rotor, especially in solid rotors. One can prevent the flux-density harmonics by making smaller stator slots. One can also use a two-layer winding and pitch the upper winding. Using this, we can eliminate high-frequency components injecting to the rotor. One way to reduce the air-gap harmonics is also to make a bigger air gap. But the side effect of the bigger air gap is naturally a bigger magnetization current.

Rotor can be a solid one or a laminated one. If the machine is a permanent-magnet synchronous machine, there will only be harmonics which induce eddy currents. The case is different with a high-speed induction machine because there is a slip. High-frequency components make the slip frequency very high. And this induces circulating currents and rotor losses. So, the use of the laminated rotor is preferred, if mechanical constraints are not very strict.

2.3 Losses in a high-speed electrical machine

Losses are essential in the thermal modelling of a high-speed electrical machine. The losses of the motor are generated according to Equation 2.1.

$$P_{\text{loss}} = k_0 + k_1\omega + k_2\omega^2 + k_3\omega^3 \tag{2.1}$$

where k_0, k_1, k_2 and k_3 are the coefficients for the resistive losses caused by the fundamental components of the stator and rotor currents, hysteresis losses in the iron core, eddy current losses in the conductors, iron core and frame and friction losses, respectively.

Comparing the losses generated in a 50 Hz machine to those generated in a high-speed machine, there is a major difference between them. The loss distribution is different. In high-speed machines, the friction, cooling and bearing losses are the major part of the losses. They increase as a function of a speed. In the 50 Hz machine, the major losses are the resistive losses. The losses between the 50 Hz machine and a high-speed machine are illustrated and compared in Figure 2.2.

2.4 Cooling methods

The role of the cooling is to remove the losses generated in the motor. The insulation class of the motor is determined by manufacturer. After this, the maximum temperature rise is fixed and the needed cooling is determined. The cooling in high-speed machines is normally an open-circuit cooling. It means that the cooling fluid flows through the machine and keeps the temperature in the air-space low. The friction losses in a high-speed machine are significant so a closed-circuit cooling is not used. Cooling can be increased with radial or axial cooling ducts.

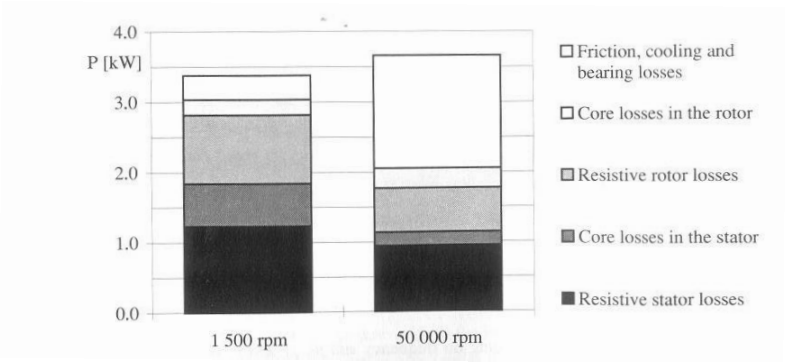

Figure 2.2: A conventional machine and a high-speed machine with the same power. The difference in the losses between a 50 Hz machine and a high-speed machine is significant.*

But cooling ducts weaken the mechanical strength and make more friction losses.

Furthermore, we can use different kinds of cooling materials. Air is used but we can also use hydrogen or helium. The advantage of these liquids is that their mass densities are low so they produce less friction losses. The disadvantage of hydrogen is that it is a hazardous gas. Liquids are also used in the cooling. One way to cool the machine is to use a heat pipe inside the rotor. The heat pipes are filled with water or alcohol and liquid vaporizes in the hot rotor thus moving heat out of the rotor.

*Lähteenmäki (2002, p.24)

Chapter 3

Convection

Convection is a phenomenon in which heat is transferred between solid and fluid domains. In electrical machines, convection is mainly the phenomenon transporting heat out from the machine. We have two kinds of convections. Natural convection is due to differences in fluid densities. For example, heat is transferred to air from a radiator. On the contrary, forced convection happens due to a forced fluid flow. For example, one can extract heat out from a circuit board by blowing air above the board. Incropera and De Witt (1990) explain the theory of the convection phenomenon in the following extracts.

A typical convection heat-transfer problem is described in Figure 3.1. We have a steady flow of the fluid flowing with the velocity V and the temperature T_∞. A local convection coefficient is h. The flow meets an arbitrary object or a flat plate with the surface temperature T_S. Because there is a temperature difference between the surface and the flow, there will happen convection. So, heat is transferred between the solid domain and the fluid.

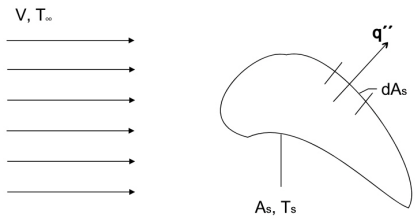

Figure 3.1: A typical convection heat-transfer problem.

The definition of a local heat flux is

$$q'' = h(T_\mathrm{s} - T_\infty) \tag{3.1}$$

The total heat-transfer rate q can be calculated by integrating the local flux q'' over the entire surface A_s

$$q = (T_\mathrm{s} - T_\infty) \int_{A_\mathrm{s}} h \, dA_\mathrm{s}. \tag{3.2}$$

Defining an average convection coefficient $\overline{h}$ for the entire surface, the total heat-transfer rate may be expressed as

$$q = \overline{h} A_\mathrm{s} (T_\mathrm{s} - T_\infty). \tag{3.3}$$

Equating equations above we get

$$\overline{h} = \frac{1}{A_\mathrm{s}} \int_{A_\mathrm{s}} h \, dA_\mathrm{s}. \tag{3.4}$$

This is a dependence between the average heat-transfer coefficient $\bar{h}$ and the local heat-transfer coefficient h.

3.1 Convection boundary layers

3.1.1 The velocity boundary layer

The velocity boundary layer is built up whenever there is a fluid flow along a surface. We can consider that fluid particles assume a zero velocity on the surface. On the other hand, the velocity above the surface reaches the free stream velocity of u_∞. One can consider that there is always a layer which slows down the next layer. The velocity boundary layer is formed. Retardation of a fluid motion is associated with shear stresses τ acting in planes that are parallel to the velocity. The development of the velocity boundary layer over a flat plate is presented in Figure 3.2.

The boundary layer thickness δ_v is defined as the height y when the fluid flow u reaches 99 % of the free stream velocity u_∞,

$$\delta_v = y|_{u=0.99u_\infty}. \tag{3.5}$$

Another important parameter is the local friction coefficient, which is

$$C_\mathrm{f} = \frac{\tau_\mathrm{s}}{\rho u_\infty^2 / 2} \tag{3.6}$$

where ρ is the density of the fluid, u_∞ is the free stream velocity and τ_s is the surface shear stress. This is a key dimensionless parameter from which the surface frictional drag may be determined.

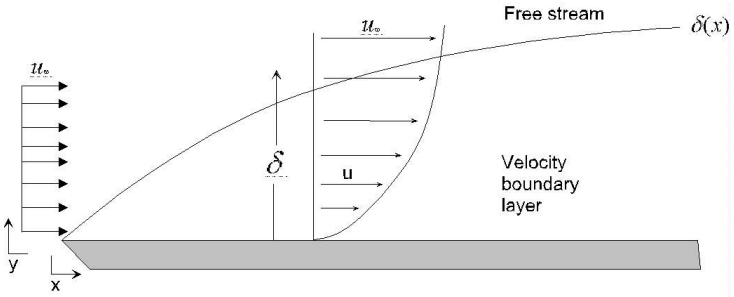

Figure 3.2: The velocity boundary layer development over a flat plate.

3.1.2 The thermal boundary layer

Like the velocity boundary layer, the thermal boundary layer is also developed. The development of the thermal boundary layer is described in Figure 3.3. The thermal boundary layer is developed whenever there is a temperature difference between the fluid and the surface. So, fluid particles that make contact with the surface have the surface temperature. In turn, these particles exchange energy with those particles in the adjoining layers and temperature gradients develop in the fluid. The thickness of the layer, δ_T, can be defined and it is the height y when

$$\delta_T = y|_{\frac{T_S - T}{T_S - T_\infty} = 0.99.} \tag{3.7}$$

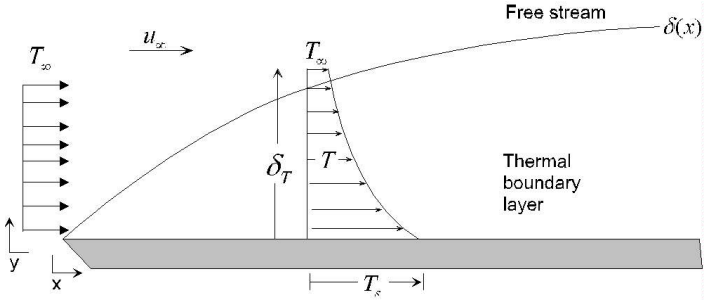

Figure 3.3: The thermal boundary layer development over a flat plate.

3.2 Laminar and turbulent flow

An essential task in heat-transfer problems is to determine whether the flow is laminar or turbulent. Consider the flow going on a flat surface. First the flow is laminar, but after some distance x_c the flow becomes turbulent and the flow is dispersed.

Figure 3.4 shows how the laminar flow becomes turbulent after some distance.

Between the laminar and the turbulent flow there is a small transition region where both laminar and turbulent flows are present. In laminar flow, the particles are going into direction parallel to the surface. The laminar flow follows the silhouette of the object. On the contrary, the turbulent flow is very irregular and roiling. It can be characterized by velocity fluctuations. The turbulent flow does not follow the surface anymore but separates from the surface.

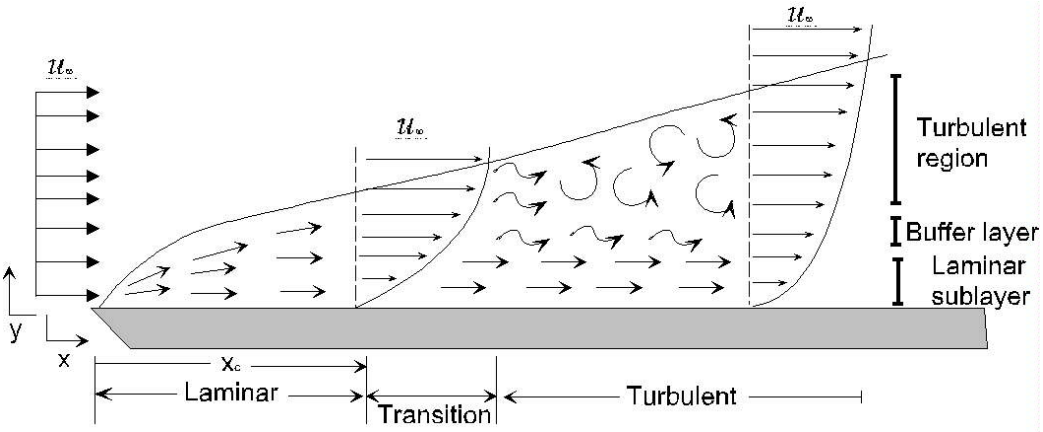

Figure 3.4: Behavior of the flow over a flat surface. X_C is the distance at which the transition to turbulent flow begins.

3.3 Dimensionless numbers

Convection heat-transfer problems are usually treated with dimensionless numbers. In this section, the most used dimensionless numbers are presented.

3.3.1 The Reynolds number

The transition from laminar to turbulent flow begins after a critical distance x_c. This distance is determined by a dimensionless grouping of variables called the Reynolds number. The Reynolds number is the ratio of inertia to viscous forces and describes how turbulent the flow is. The definition is

$$Re = \frac{vL}{\mu}. \tag{3.8}$$

where L is the characteristic dimension of the body, v is the velocity of the fluid and μ is the dynamic viscosity of the fluid. The critical Reynolds number Re_c is the value where the transition begins. If the Reynolds number is lower than Re_c, the flow will remain laminar. If the value is bigger than Re_c, the flow is turbulent.

The Reynolds number is different for different kind of surfaces. The value also depends on the surface roughness and the turbulence level of the free stream. The critical Reynolds number for a flat plate is $5 \cdot 10^5$.

3.3.2 The Nusselt number

Another important number is the Nusselt number. The Nusselt number is a dimensionless measure of the heat-transfer coefficient for different fluid flows. The definition is

$$Nu = \frac{hL}{k_\mathrm{f}} \tag{3.9}$$

where h is the heat-transfer coefficient, L is the characteristic dimension and k_f is the thermal conductivity of the fluid.

3.3.3 The Prandtl number

The Prandtl number is the ratio of momentum and thermal diffusivities and its definition is

$$Pr = \frac{c_p \mu}{k_\mathrm{f}} \tag{3.10}$$

where c_p is the specific heat of the fluid, μ is the dynamic viscosity of the fluid and k_f is the thermal conductivity of the fluid. The Prandtl number describes static properties of the fluid substance.

3.3.4 The Grashof number

The Grashof number is the ratio of buoyancy to viscous forces and its definition is

$$Gr = \frac{\rho^2 \mathrm{g} \beta (T_s - T_\infty) d_\mathrm{h}^3}{\mu^2} \tag{3.11}$$

where ρ is the density of the fluid, g is the gravitational acceleration, β is the volumetric thermal-expansion coefficient of the fluid, $(T_s - T_\infty)$ is the temperature difference between the surface and the fluid, μ is the dynamic viscosity of the fluid and d_h is the characteristic dimension of the body. The Grashof number is used to determine the amount of the natural convection in the fluid flow.

3.4 The effects of turbulence

The Reynolds number determines whether the fluid is laminar or turbulent. A small Reynolds number means that the flow is laminar and disturbances in the flow are dissipated. When the Reynolds number is big enough, fluctuations will

be amplified and the flow will be turbulent.

Mathematically it is not easy to describe the turbulent flow. However, we can present the velocity or the temperature of the turbulent flow with an equation

$$P = \overline{P} + P' \tag{3.12}$$

where $\overline{P}$ is the average value of P and P' is the fluctuating component of the fluid. So, properties can be described with an average and a fluctuating component, as described in Figure 3.5. Because of these small fluctuating components, the heat-transfer coefficient of the turbulent flow is enhanced compared to the laminar flow. This is described in Figure 3.6. The boundary layers of the laminar and turbulent flows are also different. The enhanced mixing of molecules makes boundary profiles more uniform compared to the laminar ones.

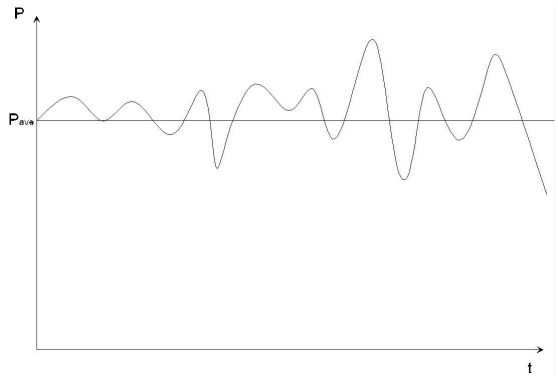

Figure 3.5: Turbulent flow properties can be described with an average and a fluctuating component.

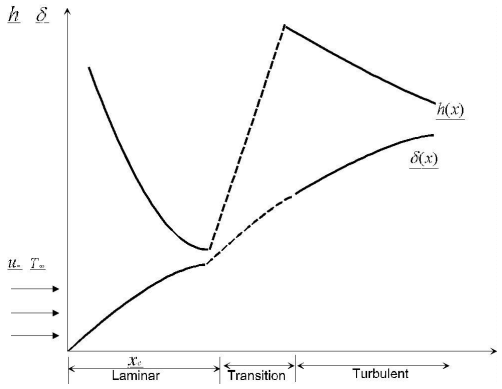

Figure 3.6: The local heat-transfer coefficient over a flat surface. Notice the increase in the coefficient as the flow becomes turbulent!

Chapter 4

Convection for different geometries

4.1 Cylinder in cross flow

Previously we have mainly observed convection over a flat plate. There are also different geometries which should be observed. Flows over different geometries are researched comprehensively, (Wagner 1988). A cylinder in cross flow is an interesting case. In the beginning, the flow will be affected by a negative pressure gradient which accelerates the flow. But after a midway, the pressure gradient changes and the flow will decelerate. Eventually, the velocity will become zero. This place on the surface is called the separation point. The velocity on the surface is reversed and is now pointing towards the front-end. The flow cannot follow the surface anymore but separates on the surface and a wake is formed. The separation is described in Figure 4.1b.

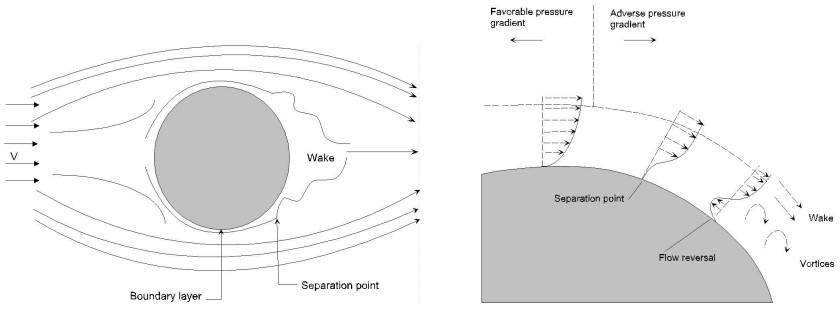

(a) *(b)*

Figure 4.1: A cylinder in cross flow.

The separation point is also affected by the Reynolds number or a turbulence. The Reynolds number for a cylinder in cross flow is

$$Re_D = \frac{\rho V D}{\mu} \tag{4.1}$$

where the characteristic length for a cylinder is the diameter D, ρ is the density of the fluid, V is the velocity of the fluid and μ is the dynamic viscosity of the fluid.

The occurrence of the separation is delayed if there is any turbulence. That is because the momentum in a turbulent boundary layer is larger than in the laminar boundary layer. If the $Re_D \lesssim 2 \cdot 10^5$, the boundary layer remains laminar and the separation occurs in $\theta \approx 80\,^\circ$. When the $Re_D \gtrsim 2 \cdot 10^5$, the boundary layer transition occurs and the separation is delayed to $\theta \approx 140\,^\circ$. The effect is described in Figure 4.2.

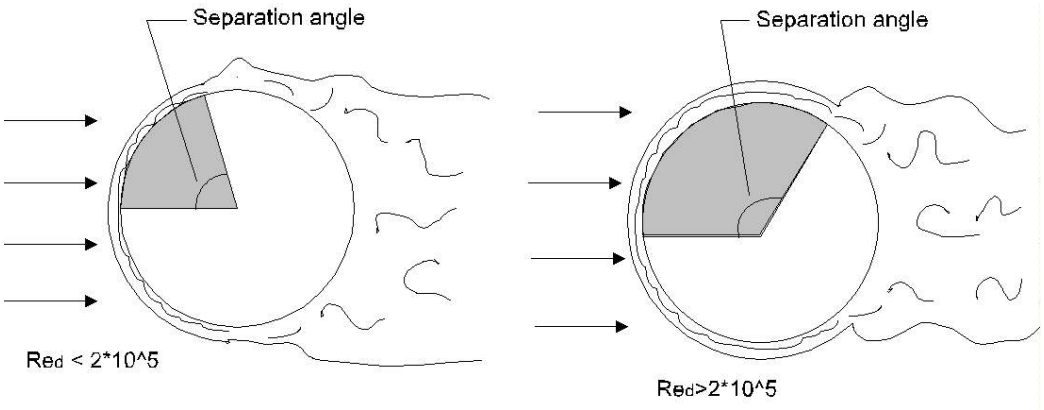

Figure 4.2: The effect of turbulence on the separation angle.

4.2 Flow in a circular tube

4.2.1 Boundary layers

This is a case of an internal flow. Like in a flow over a flat surface, a velocity boundary layer will also develop into a tube. This time the boundary layer is different because there are surfaces surrounding the fluid. The velocity boundary will develop with the increasing x until there happens merger with surrounding boundary layers. After that, the boundary layer will no longer develop. The flow is said to be fully developed. The fully developed velocity profile is parabolic. Until the fully developed region is reached, the boundary layer is called a hydrodynamic entrance region.
The thermal boundary layer is also developed. It is depicted in Figure 4.3. If the fluid enters the tube with a uniform temperature $T(r, 0)$, which is less than

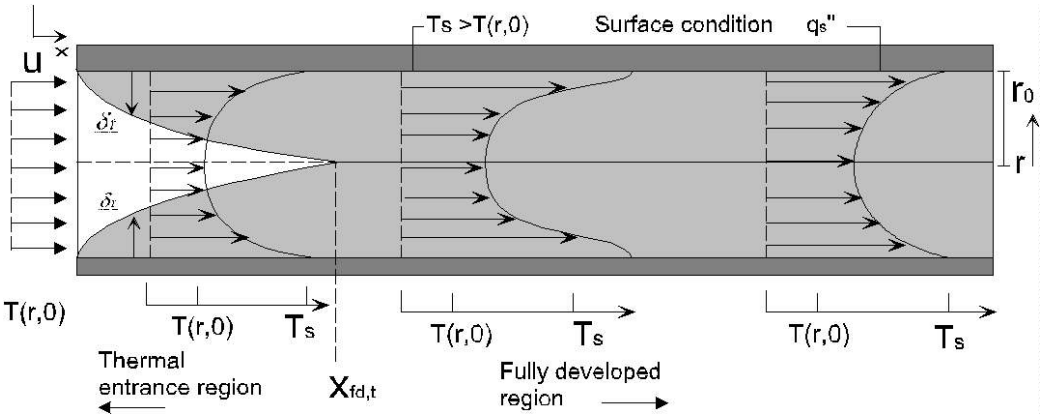

Figure 4.3: Development of the thermal boundary layer in the tube.

the surface temperature, there will happen convection. The thermal boundary layer will develop similarly like the velocity boundary layer. The thermal entrance region is the region where the boundary layer is not yet totally developed. For laminar flow, the thermal entry length $x_{\mathrm{fd,t}}$ may be expressed as

$$(\frac{x_{\mathrm{fd,t}}}{D})_{\mathrm{lam}} \approx 0.05 Re_D Pr. \tag{4.2}$$

The fully developed region is developed when the thermal boundary layers merge after a distance. We are using the mean temperature T_{m} when dealing with internal flows. The free flow temperature T_∞ of external flows represents same as the mean temperature for the internal flow. The free flow temperature T_∞ is a constant in the flow direction but the mean temperature T_{m} of the internal flow is not. The mean temperature of the fluid is defined by the thermal energy which is transported over the tube cross section. This transport is happening by the rate $\dot{E}_{\mathrm{t}}$ and it is obtained by integrating the product of the mass flux (ρu) and the internal energy per unit mass ($c_v T$) over the cross-section A_{C}

$$\dot{E}_{\mathrm{t}} = \int_{A_{\mathrm{C}}} \rho u c_v T dA_{\mathrm{C}}. \tag{4.3}$$

The mean temperature can be defined such that

$$\dot{E}_t \equiv \dot{m} c_v T_{\mathrm{m}} \tag{4.4}$$

from which we get

$$T_{\mathrm{m}} = \frac{\int_{A_{\mathrm{C}}} \rho u c_v T dA_{\mathrm{C}}}{\dot{m} c_v}. \tag{4.5}$$

4.2.2 Fully developed conditions

We can define a dimensionless temperature difference B. This is

$$B = \frac{T_\mathrm{s} - T}{T_\mathrm{s} - T_\mathrm{m}} \tag{4.6}$$

where T_s is the tube surface temperature, T is the local fluid temperature and T_m is the mean temperature of the fluid. The flow is said to be thermally fully developed when the profile no longer changes. Formally, it is stated as

$$\frac{\partial}{\partial x}[\frac{T_\mathrm{s}(x) - T(r,x)}{T_\mathrm{s}(x) - T_\mathrm{m}(x)}]_\mathrm{fd,t} = 0. \tag{4.7}$$

This condition is eventually reached in a tube for which there is either a uniform surface temperature or a uniform surface heat flux. The uniform surface heat flux can be reached if the wall of the tube is heated electrically. The uniform surface temperature can be reached when the phase change is occurring at the outer surface. However, it is impossible to impose these phenomena simultaneously. From Equation 4.7 we can realize important things. The temperature ratio is independent of x and because of that the derivative of this ratio respect to r must also be independent of x. We can obtain following equations by evaluating this derivative on the tube surface. T_s and T_m are constants because the differentiation with respect to r is concerned

$$\frac{\partial}{\partial r}(\frac{T_\mathrm{s} - T}{T_\mathrm{s} - T_\mathrm{m}})|_{r=r_0} = \frac{-\partial T/\partial r|_{r=r_0}}{T_\mathrm{s} - T_\mathrm{m}} \neq f(x). \tag{4.8}$$

Substituting for $\partial T/\partial r$ from the Fourier's law which is of the form

$$q_s'' = -\mathrm{k}\frac{\partial T}{\partial y}|_{y=0} = \mathrm{k}\frac{\partial T}{\partial r}|_{r=r_0} \tag{4.9}$$

and for q_s'' from the Newton's law of cooling which is

$$q_\mathrm{s}'' = h(T_\mathrm{s} - T_\mathrm{m}), \tag{4.10}$$

we obtain

$$\frac{h}{\mathrm{k}} \neq f(x) \tag{4.11}$$

So, in the thermally developed flow of the fluid with constant properties, the local convection coefficient h is a constant, independent of x. The local heat-transfer coefficient h is depicted as a function of the tube length in Figure 4.4.

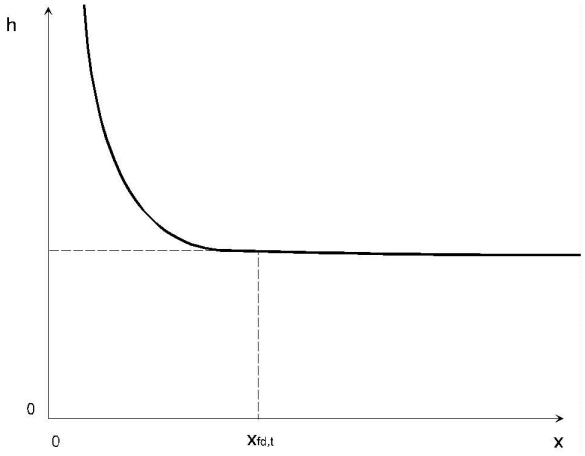

Figure 4.4: Local convection coefficient is a constant in a tube when the flow is thermally fully developed.

4.2.3 Constant surface heat flux

The surface heat flux q_s'' is a constant and independent of x over the surface. The total heat-transfer rate is

$$q_{\text{conv}} = q_s''(P \cdot L) \tag{4.12}$$

where L is the length of the tube and P is the surface perimeter ($P = \pi D$ for a circular tube). We can write for the entire tube the following equation

$$q_{\text{conv}} = \dot{m} c_p (T_{\text{m,0}} - T_{\text{m,i}}) \tag{4.13}$$

where q_{conv} is the total tube heat-transfer rate, $\dot{m}$ is the constant fluid flow rate, c_p is the gas constant, $T_{\text{m,o}}$ and $T_{\text{m,i}}$ are the tube outlet and inlet mean temperatures, respectively. Using Equation 4.13 and Equation 4.10, we can get the following equation

$$\frac{dT_{\text{m}}}{dx} = \frac{q_s'' P}{\dot{m} c_p} = \frac{P}{\dot{m} c_p} h(T_{\text{s}} - T_{\text{m}}). \tag{4.14}$$

Because the heat flux q_s'' is a constant, it also follows that right-hand side of Equation 4.14 is a constant and independent of x. Thus

$$\frac{dT_{\text{m}}}{dx} = \frac{q_s'' P}{\dot{m} c_p} \neq f(x). \tag{4.15}$$

Integrating from $x = 0$, it follows that

$$T_{\text{m}} = T_{\text{m,i}} + \frac{q_s'' P}{\dot{m} c_p}. \tag{4.16}$$

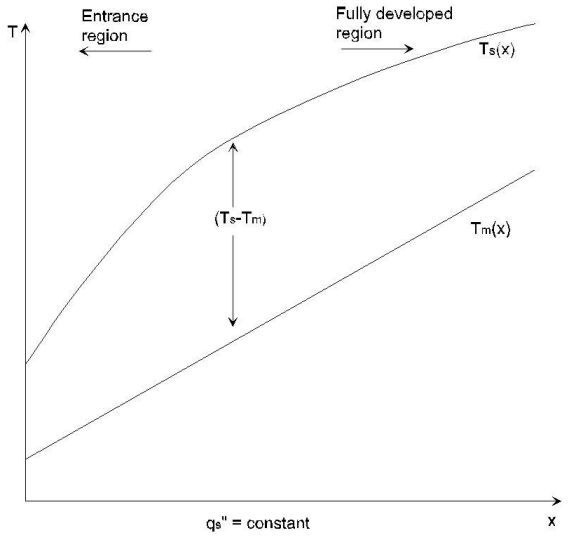

Figure 4.5: Behavior of the surface and the mean temperature when the surface heat flux is a constant.

The result is depicted in Figure 4.5. So, the mean temperature varies linearly with the x along the tube. Also from the Newton's law of cooling we can see that the temperature difference $(T_\mathrm{s} - T_\mathrm{m})$ varies with x. The difference is initially small due to the large value of h at the entrance. But it increases with increasing x due to decrease in h that occurs as the boundary layer develops. However, in the fully developed region $(T_\mathrm{s} - T_\mathrm{m})$ is a constant. That is because h is independent of x in this region.

4.2.4 Constant surface temperature

The surface temperature is a constant T_s. We can define $T_\mathrm{s} - T_\mathrm{m}$ as ΔT. Now we can express Equation 4.14 as

$$\frac{dT_\mathrm{m}}{dx} = -\frac{d(\Delta T)}{dx} = \frac{P}{\dot{m}c_p h \Delta T} \tag{4.17}$$

Separating the variables and integrating from the tube inlet to the outlet,

$$\int_{\Delta T_\mathrm{i}}^{\Delta T_\mathrm{o}} \frac{d(\Delta T)}{\Delta T} = -\int_0^L \frac{P}{\dot{m}c_p} h dx \tag{4.18}$$

or

$$\ln\frac{\Delta T_\mathrm{o}}{\Delta T_\mathrm{i}} = -\frac{PL}{\dot{m}c_p}\left(\int_0^L \frac{1}{L} h dx\right) \tag{4.19}$$

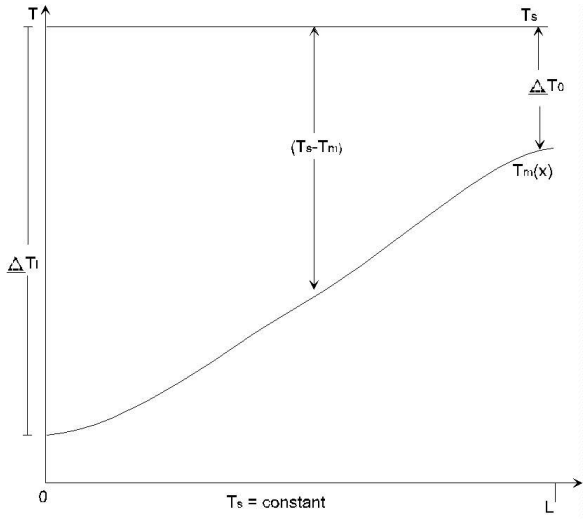

Figure 4.6: Behavior of the surface and the mean temperature when the surface temperature is a constant.

and from the definition of the average convection heat-transfer coefficient, it follows that

$$\ln\frac{\Delta T_{\mathrm{o}}}{\Delta T_{\mathrm{i}}} = -\frac{PL}{\dot{m}c_p}\bar{h_{\mathrm{L}}} \tag{4.20}$$

where $\bar{h_{\mathrm{L}}}$ is the average value of h for the entire tube. If we integrate equation to some axial x within the tube, we obtain general result for a tube with a constant surface temperature of T_{s}.

$$\frac{T_s - T_{\mathrm{m}}(x)}{T_{\mathrm{s}} - T_{\mathrm{m,i}}} = \exp(-\frac{Px}{\dot{m}c_p}\bar{h_{\mathrm{L}}}). \tag{4.21}$$

So, the temperature difference $(T_{\mathrm{s}} - T_{\mathrm{m}})$ decays exponentially with the distance along the tube, as depicted in Figure 4.6.

4.2.5 Temperature distribution in the fully developed region

The energy equation for the fully developed region in cylinderical coordinates is

$$u\frac{\partial T}{\partial x} + \nu\frac{\partial T}{\partial r} = \frac{\alpha}{r}\frac{\partial}{\partial r}(r\frac{\partial T}{\partial r}) \tag{4.22}$$

where α is the thermal diffusivity of the fluid, u and v are the velocity components along and parallel the surface, respectively. We can reduce Equation 4.22 by substituting the temperature gradient and axial velocity component.

$$\frac{\partial T}{\partial x}|_{\mathrm{fd,t}} = \frac{\partial T_m}{dx}|_{\mathrm{fd,t}} \tag{4.23}$$

$$\frac{u(r)}{u_m} = 2[1 - (\frac{r}{r_0})^2] \tag{4.24}$$

$$\frac{1}{r}\frac{d}{dr}(r\frac{dT}{dr}) = \frac{2u_\mathrm{m}}{\alpha}(\frac{dT_\mathrm{m}}{dx}[1 - \frac{r}{r_0}^2]) \tag{4.25}$$

where $(2u_\mathrm{m}/\alpha)(dT_\mathrm{m}/dx)$ is a constant. Now we can separate the variables and integrate twice to get an expression for the radial temperature distribution

$$T(r) = \frac{2u_\mathrm{m}}{\alpha}(\frac{dT_\mathrm{m}}{dx})[\frac{r^2}{4} - \frac{r^4}{16r_0^2}] + \mathrm{C}_1 + \mathrm{C}_2. \tag{4.26}$$

The constants can be solved by applying proper boundary conditions. The temperature at $r = 0$ is finite and it follows that $\mathrm{C}_1 = 0$. C_2 can be solved from the requirement $T(r_0) = T_\mathrm{s}$ and it is

$$\mathrm{C}_2 = T_\mathrm{s} - \frac{2u_\mathrm{m}}{\alpha}(\frac{dt_\mathrm{m}}{dx})(\frac{3r_0^2}{16}). \tag{4.27}$$

The temperature profile for the fully developed region with a constant surface heat flux is

$$T(r) = T_\mathrm{s} - \frac{2u_\mathrm{m}r_0^2}{\alpha}(\frac{dT_\mathrm{m}}{dx})[\frac{3}{16} + \frac{1}{16}\frac{r}{r_0} - \frac{1}{4}\frac{r}{r_0^2}]. \tag{4.28}$$

4.2.6 The constant Nusselt number

From Equation 4.14, where $P = \pi D$ and $\dot{m} = \rho u_\mathrm{m}(\pi D^2/4)$, we obtain

$$T_\mathrm{m} - T_\mathrm{s} = -\frac{11}{48}\frac{q_\mathrm{s}'' D}{\mathrm{k_f}}. \tag{4.29}$$

Combining Equation 4.29 and Newton's law of cooling, Equation 4.10, we obtain

$$h = \frac{48}{11}(\frac{\mathrm{k_f}}{D}) \tag{4.30}$$

or

$$Nu_D = \frac{hD}{\mathrm{k_f}} = 4.36. \tag{4.31}$$

So, in the circular tube characterized by uniform surface heat flux and laminar, fully developed conditions, the Nusselt number is a constant. It is independent of Re_D, Pr and axial location x.

4.3 Convection correlations

4.3.1 A turbulent flow

We have not yet spoken about turbulent flows in tubes. Convection correlations are used for turbulent flows in tubes. Here are mentioned some and you may find many more from the literature. The Colburn equation is

$$Nu_D = 0.023 Re_D^{4/5} Pr^{1/3}. \tag{4.32}$$

The Dittus-Boelter equation is a slightly different version of the above and is of the form

$$Nu_D = 0.023 Re_D^{4/5} Pr^{\mathrm{n}} \tag{4.33}$$

where n=0.4 is for heating and n=0.3 for cooling. These equations are valid in the range of conditions

$$\begin{aligned} 0.7 &\leq Pr \leq 160 \\ Re_D &\gtrsim 10000 \\ \frac{L}{D} &\gtrsim 10 \end{aligned}$$

These equations should be used for small to moderate differences, $T_\mathrm{s} - T_\mathrm{m}$, with all the properties evaluated at T_m. For flows with large property variations, the following Sieder and Tate equation should be used

$$Nu_D = 0.027 Re_D^{4/5} Pr^{1/3} (\frac{\mu}{\mu_\mathrm{s}})^{0.14} \tag{4.34}$$

where μ is the dynamic viscosity of the fluid and μ_s is the dynamic viscosity of the fluid at the surface temperature. These equations are valid in the range of conditions

$$\begin{aligned} 0.7 &\leq Pr \leq 16700 \\ Re_D &\gtrsim 10000 \\ \frac{L}{D} &\gtrsim 10 \end{aligned}$$

where all the properties, except μ_s, are evaluated at T_m. The foregoing correlations may be applied for both the constant surface temperature and the constant heat-flux conditions.

Another correlation, which is widely used and attributed to Petukhov, Kirillov and Popov, is of the form

$$Nu_D = \frac{(f/8)Re_D Pr}{1.07 + 12.7(f/8)^{1/2}(Pr^{2/3} - 1)} \tag{4.35}$$

where friction factor f can be obtained from the Moody diagram (Appendix A) or for smooth tubes from the expression

$$f = (1.82\log_{10}Re_D - 1.64)^{-2}. \tag{4.36}$$

The correlation is valid for $0.5 < Pr < 2000$ and $10^4 < Re_D < 5 \cdot 10^6$. For smaller Reynolds numbers, Gnielinski modified the correlation and proposed an expression of the form

$$Nu_D = \frac{(f/8)(Re_D - 1000)Pr}{1 + 12.7(f/8)^{1/2}(Pr^{2/3} - 1)} \tag{4.37}$$

where for smooth tubes, the friction is given by

$$f = (0.79\ln Re_D - 1.64)^{-2}. \tag{4.38}$$

The correlation is valid for $0.5 < Pr < 2000$ and $2300 < Re_D < 5 \cdot 10^6$. For both equations, the properties should be evaluated at T_m.

From all these equations we notice that the first two are only for smooth tubes. For turbulent flow, the heat-transfer coefficient can be enhanced with wall roughness. The latter two equations are with friction factors. Friction factor can be obtained from the Moody diagram (Appendix A). We can increase h by increasing f. However the increase in f is proportionately larger, and when f is approximately four times larger than the corresponding value for a smooth surface, h no longer changes with additional increases in f.

Entry lengths for turbulent flows are typically short, $10 \leq (x_\mathrm{fd}/D) \leq 60$. For that reason, it is reasonable to assume that the average Nusselt number for the entire tube is equal to the value associated with the fully developed region, $\overline{Nu_D} \approx Nu_{D,\mathrm{fd}}$. For short tubes, $\overline{Nu_D}$ will exceed $Nu_{D,\mathrm{fd}}$ and may be calculated from an expression of the form

$$\frac{\overline{Nu_D}}{Nu_{D,\mathrm{fd}}} = 1 + \frac{\mathrm{C}}{(x/D)^\mathrm{m}} \tag{4.39}$$

where C and m depend on the nature of the inlet (sharp-edged or nozzle) and from the entry region (thermal or combined) and also on the Prandtl number and on the Reynolds number. Typically, errors of less than 15% are associated with assuming $\overline{Nu_D} = Nu_{D,\mathrm{fd}}$ for $(L/D) > 60$.

4.3.2 Noncircular cross-section

Many technical applications involve tubes with a noncircular cross-section. However, for these tubes we can use effective diameter as a characteristic length. It is called a hydraulic diameter and is defined as

$$D_{\mathrm{h}} = \frac{4A_{\mathrm{c}}}{P} \tag{4.40}$$

where A_{c} is the flow cross-sectional area and P is the wetted perimeter. This diameter should be used when calculating parameters such as Re_D and Nu_D.
For laminar flow, the use of the correlation is less accurate, particularly with cross sections characterized by sharp corners. For such cases, the Nusselt number corresponding to fully developed conditions can be obtained from Table 4.1. This table is based on solutions of the differential momentum and energy equations for flow through the different duct cross sections. Many other cross-sections are discussed in the work of Shah and London (1978).

Table 4.1: Nusselt numbers for fully developed laminar flow in tubes of differing cross section.*

CROSS SECTION	$\frac{b}{a}$	$Nu_D \equiv \frac{hD_h}{k}$ (uniform q_s'')	$Nu_D \equiv \frac{hD_h}{k}$ (uniform T_s)
	—	4.36	3.66
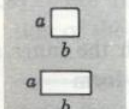	1.0	3.61	2.98
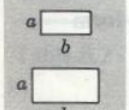	1.43	3.73	3.08
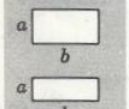	2.0	4.12	3.39
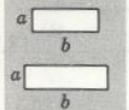	3.0	4.79	3.96
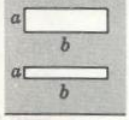	4.0	5.33	4.44
	8.0	6.49	5.60
	∞	8.23	7.54
	—	3.11	2.47

*Incropera and De Witt (1990, p.501)

Chapter 5

Determination of heat-transfer coefficients using empirical methods

Average heat-transfer coefficients of a high-speed machine can be calculated using traditional empirical methods. Saari (1995) presents equations for a calculation of the average heat-transfer coefficient $\bar{h}$. The high-speed machine is divided in different areas or geometries. In Figure, 5.1 different sections of the machine are presented. Every area of the machine is treated as a particular geometry and the Nusselt number is calculated for every section of the machine which gives us the average heat-transfer coefficient. There are several convection correlations for the Nusselt number Nu. The average heat-transfer coefficient can be obtained and it is

$$h = \frac{k_{\mathrm{f}} Nu}{l} \tag{5.1}$$

where k_{f} is the thermal conductivity of the fluid and l is the characteristic dimension of the geometry.

5.1 Heat transfer in the air gap

The air gap is very important for the cooling of the electrical machine. The fluid in the air gap removes the heat which is generated in the rotor and also some part of stator losses. It also removes friction losses. The heat-transfer coefficient depends on fluid properties, the rotation speed, the axial cooling flow, air-gap dimensions and surface qualities. The air-gap is considered as a channel between concentrated cylinders and its Nusselt number is

$$Nu = \frac{h\delta}{k_{\mathrm{f}}} \tag{5.2}$$

where δ is the radial air-gap length, h is the heat-transfer coefficient for one air-gap

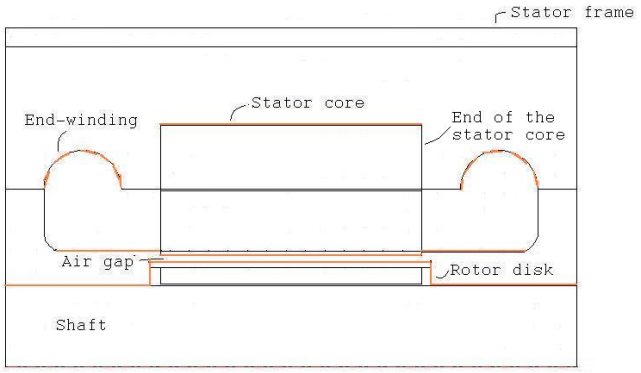

Figure 5.1: Axisymmetric geometry of the high-speed machine and different sections of the machine.

surface (rotor or stator) and k_f is the thermal conductivity of the fluid.

The rotating rotor forces the fluid to a tangential movement and induces toroidal vortices. This toroidal movement is referred to the Taylor-vortex flow. The flow in the air-gap is different compared to the flow between two parallel plates. The Taylor vortices are described by the Taylor number.

$$Ta = \frac{\rho^2 \omega^2 r_\mathrm{m} \delta^3}{\mu^2} \tag{5.3}$$

where ω is the angular velocity, r_m is the average of the stator and rotor radii, δ is the length of the air gap, ρ is the density of the fluid and μ is the dynamic viscosity of the fluid. The modified Taylor number takes into account the rotor radius and the radial air-gap length:

$$Ta_\mathrm{m} = \frac{Ta}{F_\mathrm{g}} \tag{5.4}$$

where F_g is the geometrical factor defined by

$$F_\mathrm{g} = \frac{\pi^4}{1697(1 - \frac{\delta}{2r_\mathrm{m}})^2 P_\mathrm{g}} \tag{5.5}$$

where

$$P_\mathrm{g} = \frac{0.00056 + 0.0571(\frac{2r_\mathrm{m} - 2.304\delta}{2r_\mathrm{m}} - \delta)}{(\frac{2r_\mathrm{m} - 2.304\delta}{2r_\mathrm{m} - \delta})}. \tag{5.6}$$

Actually, the radial air-gap length is so small compared with the rotor radius that the value of F_g is close to unity and therefore $Ta_\mathrm{m} \sim Ta$.

There have been several studies about the heat transfer in the air gap. The Nusselt number in the air gap has been measured by many researchers, (Gazley, 1958 cited in Saari, 1995, p.36), (Bjorklund et al., 1959 cited in Saari, 1995, p.36) and (Becker et al., 1962 cited in Saari, 1995, p.36). The air gap flow depends on the modified Taylor number and it can be divided into three regions:

$$Nu = 2 \qquad (Ta_{\mathrm{m}} < 1700) \tag{5.7}$$

$$Nu = 0.128 Ta_{\mathrm{m}}^{0.367} \qquad (1700 < Ta_{\mathrm{m}} > 10^4) \tag{5.8}$$

$$Nu = 0.409 Ta_{\mathrm{m}}^{0.241} \qquad (10^4 < Ta_{\mathrm{m}} > 10^7). \tag{5.9}$$

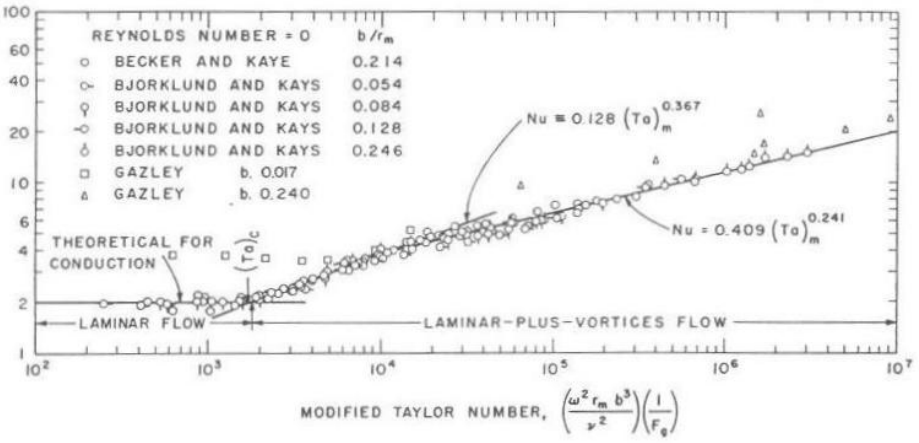

Figure 5.2: Nusselt number for a tangential air-gap flows.*

Aoki et al. (1967 cited in Saari, 1995, p.37) have also made studies with different Prandtl numbers and radial air-gap lengths. Their studies were carried out with several fluids whose Prandtl numbers were from 0.7 to 160. They found that the equation

$$Nu = 0.44 Ta_{\mathrm{m}}^{0.25} Pr^{0.3} \tag{5.10}$$

fitted their experimental results best.

The above equations were obtained for rotating cylinders without any axial flow through the air gap. The axial flow delays the occurrence of Taylor vortices and decreases heat transfer at low modified Taylor numbers.

5.2 Heat transfer on the shaft surface

Heat transfer on the shaft surface is modelled in the same way as heat transfer in the air gap because the geometry is the same. So, one can use the equations

*Becker et al. (1962 cited in Saari, 1995, p.36)

5.2 to 5.10 for the calculation. The dimensions are only bigger. The air gap δ is substituted with the channel wide l which is the distance between the end winding and the shaft.

5.3 Heat transfer from the rotor disks

The end regions of the rotor can be modeled as disks. The Nusselt number for disks rotating in free space is

$$Nu = \frac{hr}{k} \tag{5.11}$$

where r is the outer radius of the disk.

The definition of the tip Reynolds number is

$$Re_{\mathrm{r}} = \frac{\rho\omega r^2}{\mu} \tag{5.12}$$

where μ is the dynamic viscosity of the fluid, ρ is the density of the fluid, ω is the angular velocity of the rotor. When the tip Reynolds number $Re_{\mathrm{r}} \geq 3 \cdot 10^5$, the flow is turbulent and the Nusselt number is

$$Nu = PrRe\frac{C_{\mathrm{m}}}{2\pi} \tag{5.13}$$

where C_{m} is the torque coefficient. The above equation is valid for compressible fluids. The definition of the torque coefficient is

$$C_{\mathrm{m}} = \frac{3.87}{Re_{\mathrm{r}}^{0.5}} \qquad (Re_{\mathrm{r}} < 3 \cdot 10^5) \tag{5.14}$$

$$C_{\mathrm{m}} = \frac{0.146}{Re_{\mathrm{r}}^{0.2}} \qquad (Re_{\mathrm{r}} > 3 \cdot 10^5) \tag{5.15}$$

5.4 Heat transfer in the end-winding space

The end-winding region can be divided in two subregions. The first one is the underside of the end winding, the surface pointing towards the shaft. The second one is the upside surface of the end-winding, pointing towards the stator frame. These two regions have different heat-transfer coefficients and fluid temperatures.

5.4.1 The underside surface

The space between the rotor and the end winding is affected by the peripheral speed of the rotor. The peripheral speeds effect on heat transfer is more than that of the cooling fluid velocity. So, the rotation speed determines the heat-transfer coefficient for the underside surface of the end winding. The geometry corresponds

to that of the air gap so we can use the equations 5.2 to 5.10. However, we can increase these figures by 40 % to 70 % because of the rough surface of the end-winding surface.

5.4.2 The upside surface

The surface between the end winding and the stator frame is more difficult to model than the space near the rotor. This is because we do not know the fluid velocity around the surface. The direction and speed of the cooling fluid is essential to the heat-transfer characteristics. We can model this area as a cylinder in cross flow. The Reynolds number is

$$Re = \frac{\rho v d}{\mu} \tag{5.16}$$

where ρ is the density of the fluid, d is the diameter of the cylinder, v is the free-stream air velocity and μ is the dynamic viscosity of the fluid. The Nusselt number for a cylinder in cross flow is

$$Nu = \mathrm{C}_1 Re^{\mathrm{C}_2} Pr^{0.33} \tag{5.17}$$

where coefficients are listed in Table 5.1.

Table 5.1: Coefficients for Equation 5.17.

Re	C_1	C_2
$0.4 - 4$	0.989	0.330
$4 - 40$	0.911	0.385
$40 - 4 \cdot 10^3$	0.683	0.466
$4 \cdot 10^3 - 4 \cdot 10^4$	0.193	0.618
$4 \cdot 10^4 - 4 \cdot 10^5$	0.027	0.805

The problem of determining the coefficient of the end-winding space is that it is not easy to determine the mean fluid temperature in the end-winding space.

5.5 Heat transfer in the end of the stator core

Ends of the stator core are difficult to model. The geometry is simple but the flow behaviour on this surface is unknown or not direct. The end-winding disturbs the cooling flow coming to this surface. Some idea for the calculation can give equations for a flat surface. The Reynolds number is

$$Re = \frac{\rho v l}{\mu} \tag{5.18}$$

where ρ is the density of the fluid, v is the mean fluid velocity, l is the radial length of the stator yoke and μ is the dynamic viscosity of the fluid. The Nusselt number for a flat surface is

$$Nu = \frac{hl}{k_{\mathrm{f}}} \tag{5.19}$$

where h is the heat-transfer coefficient, l is the radial length of the stator yoke and k_{f} is the thermal conductivity of the fluid. There are also convection correlations for the Nusselt number which are

$$Nu = 0.664 Re^{0.5} Pr^{0.33} \tag{5.20}$$

$$Nu = 0.037 Re^{0.8} Pr^{0.33} \tag{5.21}$$

for laminar and turbulent flows, respectively.

5.6 Heat transfer between the stator core and the frame

This case can be modeled as a problem of an internal flow. There are ribs between the stator frame and the stator core which holds the frame and core together. The cooling fluid is flowing in the channel between the ribs (Figure 5.3). We use a convection correlation for this problem by defining the hydraulic diameter for this cross-section,

$$D_{\mathrm{h}} = \frac{4A_{\mathrm{c}}}{P} \tag{5.22}$$

where A_{c} is the cross-section of the channel and P is the wetted perimeter of the channel. The hydraulic diameter is the characteristic dimension for the cooling channel.

The Reynolds number for the cooling channel is

$$Re = \frac{\rho u_{\mathrm{m}} D_{\mathrm{h}}}{\mu} \tag{5.23}$$

where ρ is the density of the fluid, u_{m} is the mean velocity of the fluid, μ is the dynamic viscosity of the fluid. The Nusselt number for the cooling channel is obtained from the Dittus-Boelter equation, Equation 4.33.

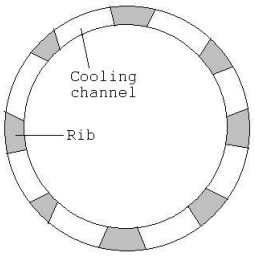

Figure 5.3: The cross-section between the stator frame and the stator core.

Chapter 6

The numerical calculation method

Earlier we had to use rough empirical methods to calculate the temperatures of a high-speed machine or a cooling fluid. The thermal-network method is a traditional method to calculate the temperature rise in the machine and in the fluid. For this, we need to model the machine and it's geometry. Pyrhönen et al. (2008) present the thermal equivalent circuit of an electrical machine.

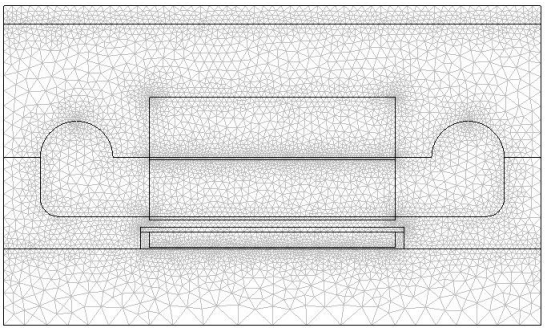

Figure 6.1: The finite element mesh of the 2D axi-symmetric geometry of the high-speed PM machine.

The developed numerical methods give us a new tool to calculate the temperature rise of the machine. The computational fluid dynamics (CFD) is the numerical way to model the coolant flow in the machine. More about modelling fluids with a finite element method are presented in literature, (Zienkiewicz et al., 2005).

6.1 The Reynolds Averaged Navier-Stokes equations

The model is two-dimensional and axi-symmetric. The flow of an incompressible fluid is described by the Reynolds Averaged Navier-Stokes equations. These equations are the basic equations for describing the movement in incompressible fluids. The Reynolds Averaged Navier-Stokes equations are

$$\rho\frac{\partial \mathbf{U}}{\partial t} - \mu\nabla\cdot\nabla\mathbf{U} + \rho\mathbf{U}\cdot\nabla\mathbf{U} + \nabla\mathbf{P} + \nabla\overline{(\rho u'\otimes u')} = \mathbf{F} \tag{6.1}$$

$$\nabla\cdot\mathbf{U} = 0 \tag{6.2}$$

where μ denotes the dynamic viscosity of the fluid, $\mathbf{U}$ is the averaged velocity field vector, u is the velocity vector, ρ is the density of the fluid, $\mathbf{P}$ is the pressure vector and $\mathbf{F}$ is the volumetric force vector. The last term on the left-hand side in the first equation represents fluctuations around the mean flow and it is called the Reynolds stress tensor. The cooling flow in a high-speed machine is typically turbulent because a turbulent flow enables better heat transfer.

6.2 κ - ϵ closure

The κ-ε turbulence model is valid for a turbulent transport at high Reynolds number. This model gives a closure to the system and results in the following equations for the conservation of momentum and continuity.

$$\rho\frac{\partial \mathbf{U}}{\partial t} - \nabla\cdot[(\mu + \rho C_\mu\frac{\kappa^2}{\epsilon})\cdot(\nabla\mathbf{U}) + (\nabla\mathbf{U})^{\mathrm{T}})] + \rho\mathbf{U}\cdot\nabla\mathbf{U} + \nabla\mathbf{P} = \mathbf{F} \tag{6.3}$$

$$\nabla\cdot\mathbf{U} = 0 \tag{6.4}$$

The two new variables in Equation 6.3 are the turbulent kinetic energy κ and the dissipation rate of the turbulent energy ϵ. Two extra equations for κ and ϵ are solved for these two introduced variables

$$\rho\frac{\partial \kappa}{\partial t} - \nabla\cdot[(\mu + \rho\frac{\mathrm{C}_\mu}{\sigma_\mathrm{k}}\frac{\kappa^2}{\epsilon})\nabla\kappa] + \rho\mathbf{U}\cdot\nabla\kappa = \rho\mathrm{C}_\mu\frac{\kappa^2}{2\epsilon}(\nabla\mathbf{U} + (\nabla\mathbf{U})^{\mathrm{T}})^2 - \rho\epsilon \tag{6.5}$$

$$\rho\frac{\partial \epsilon}{\partial t} - \nabla\cdot[(\mu + \rho\frac{\mathrm{C}_\mu}{\sigma_\epsilon}\frac{\kappa^2}{\epsilon})\nabla\epsilon] + \rho\mathbf{U}\cdot\nabla\epsilon = \rho\mathrm{C}_{\epsilon 1}\frac{\kappa}{2}(\nabla\mathbf{U} + (\nabla\mathbf{U})^{\mathrm{T}})^2 - \rho\mathrm{C}_{\epsilon 2} - \rho\mathrm{C}_{\epsilon 2}\frac{\epsilon^2}{\kappa} \tag{6.6}$$

C_μ, $\mathrm{C}_{\epsilon 1}$, $\mathrm{C}_{\epsilon 2}$, σ_κ, σ_ϵ are model constants and they are determined from the experimental data. The values for the coefficients are presented in Table 6.1.

The κ - ϵ turbulence model gives an isotropic turbulence, which is a turbulence constant in all directions.

Table 6.1: Model constants for Equation 6.6.

C_μ	$C_{\epsilon 1}$	$C_{\epsilon 2}$	σ_κ	σ_ϵ
0.09	1.44	1.92	0.9	1.3

6.3 Boundary conditions

The turbulent flow near to a solid surface is highly anisotropic and that is why we need boundary conditions represented with empirical equations. The complete set of boundary conditions for the solid wall is elaborated and the boundary conditions for κ and ϵ are respectively

$$\kappa = \frac{u_\tau}{\sqrt{C_\mu}}; \epsilon = \frac{u_\tau^3}{k_a y} \tag{6.7}$$

where u_τ is the friction velocity, $k_a \approx 0.42$ is the Karman's constant and y is the normal distance from the wall.

Besides boundary conditions, the thermal conductivity of the fluid needs to be corrected. It is corrected to take into account the effect of mixing due to eddies and is called an effective thermal conductivity:

$$k_{\text{eff}} = k_f + k_t \tag{6.8}$$

$$k_t = c_p \mu_t. \tag{6.9}$$

Here k_f is the physical thermal conductivity of the fluid, k_t is the turbulent conductivity, μ_t is the turbulent kinematic viscosity and c_p is the heat capacity of the fluid. More about thermal design of a high-speed machine is presented, (Kolondzovski et al., 2009) and (Kolondzovski et al., 2008).

6.4 Thermal wall function

When calculating the local heat-transfer coefficient, a proper heat-transfer rate q needs to be obtained, (Comsol Multiphysics, 2006). The heat-transfer application modes use the predefined group wall. The laminar sublayer is not modelled in the turbulence model.

For example, the temperature is not modelled in the laminar sublayer. Instead of assuming continuity of the temperature across the layer, a thermal "wall function" is used. There is a jump in the temperature from the solid surface to the fluid due to the omitted laminar sublayer. Taking this into account, the predefined group for the wall gives the heat flux q. The definition is

$$q = \frac{\rho c_p C_\mu^{1/4} k_w^{1/2} (T_w - T)}{T^+} \tag{6.10}$$

where ρ is the density of the fluid, c_p is the heat capacity of the fluid. C_μ is a constant of the turbulence model and k_w is the value of the turbulent kinematic energy at the wall. T_w equals the temperature of the solid at the wall and T is the temperature of the fluid on the other side of the omitted laminar sublayer.

The quantity T^+ is related to the dimensionless wall distance and has the following definition:

$$T^+ = \frac{Pr_\mathrm{T}}{\kappa}\ln(y^+) + \beta \tag{6.11}$$

with the dimensionless wall distance y^+, given by:

$$y^+ = \frac{y_\mathrm{w} C_\mu^{1/4} k_\mathrm{w}^{1/2}}{v} \tag{6.12}$$

where Pr_T is the turbulent Prandtl number, κ_a is the Karman's constant and β is the model constant.

Chapter 7

Results and discussion

The machine is a high-speed permanent magnet machine. It is designed to operate with a speed n=31500 rpm and has a power of P=130 kW. The permanent magnets are shielded by an aluminium cage which shields them from eddy-current heat generation. The carbon-fibre sleeve keeps the magnets and the aluminium cage in place during a high-speed operation when huge centrifugal forces arise.

This chapter will focus on simulations achieved with Comsol Multiphysics 3.3. These simulation results will be compared to those calculated analytically. The analytical equations used were presented in the previous chapter. The results are discussed in this chapter. Simulated heat-transfer coefficients are described and explained with the results obtained from the computational fluid dynamics. The local heat-transfer coefficients are calculated with the program from every surface as a function of a distance. The average values can be obtained from these functions. The temperature field and the velocity field can also be obtained with the simulation program. The local heat-transfer coefficients for every region are presented in figures. The inlet side coefficient is presented first and the outlet side next. The simulated values can be compared to the analytical values. The properties of air are gathered in Table 7.1.

Table 7.1: The properties of the cooling flow air.

dynamic viscosity	density	angular velocity	thermal conductivity	Prandtl number	velocity
$\mu[\frac{\mathrm{N{\cdot}s}}{\mathrm{m^2}}]$	$\rho[\frac{\mathrm{Kg}}{\mathrm{m^3}}]$	$\omega[\frac{\mathrm{rad}}{\mathrm{s}}]$	$k[\frac{\mathrm{W}}{\mathrm{mK}}]$	Pr	$v[\frac{\mathrm{m}}{\mathrm{s}}]$
$190 \cdot 10^{-3}$	1.2	3298.672	0.028	0.71	50

7.1 Heat transfer in the air gap

Analytical calculations for the average heat-transfer coefficient in the air gap gave $\overline{h_{\mathrm{em}}} \approx 270 \frac{\mathrm{W}}{\mathrm{m^2K}}$. The simulated values of the heat-transfer coefficient are shown in Figure 7.1a and in Figure 7.1b.

From Figure 7.1a and from Figure 7.1b we can see that the coefficient is generally descending from the beginning of the tube entrance and is closing to a constant value at the other side of the air gap. Both graphs resemble each other. The flow is said to be fully developed. This phenomenon and equations for this were already depicted in the previous chapter and in Figure 4.4. The peaks in the beginning and in the end are due to turbulence. The turbulence is intense in the sharp corners which induce high fluctuations to the flow. The numerical average value for the heat-transfer coefficient of stator surface was $\overline{h_{\mathrm{nu}}} \approx 254 \frac{\mathrm{W}}{\mathrm{m^2K}}$. The numerical average value of the heat-transfer coefficient for the rotor surface was $\overline{h_{\mathrm{nu}}} \approx 229 \frac{\mathrm{W}}{\mathrm{m^2K}}$. These are very close to the analytical value and proves that the analytical equations are valid for the air gap.

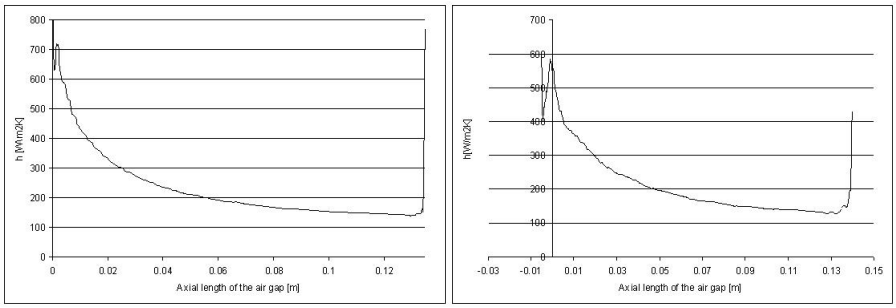

(a) The stator surface *(b)* The rotor surface

Figure 7.1: The local heat transfer coefficients in the air gap.

7.2 Heat transfer on the shaft surface

The analytical equations were the same as for the air gap. This area is modelled as two concentric cylinders. The analytical equations for the shaft gave $\overline{h_{\mathrm{em}}} \approx 147 \frac{\mathrm{W}}{\mathrm{m^2K}}$.

The simulation results are presented in Figure 7.2. The cooling fluid is flowing from the left to the right. The calculated values for the inlet and outlet average heat-transfer coefficient were $\overline{h_{\mathrm{nu}}} \approx 177 \frac{\mathrm{W}}{\mathrm{m^2K}}$ and $\overline{h_{\mathrm{nu}}} \approx 179 \frac{\mathrm{W}}{\mathrm{m^2K}}$, respectively. Both Figures show small fluctuations which are typical for a turbulent flow. The inlet heat-transfer coefficient decreases because the velocity also decreases along the shaft. Near the air gap the velocity is close to zero. In the outlet side, the velocity also varies causing the variations to the heat-transfer coefficient. The geometry is simple for the shaft. It is a simple smooth surface. It is possible to determine the average heat-transfer coefficient empirically. Only the average velocity needs to be assumed.

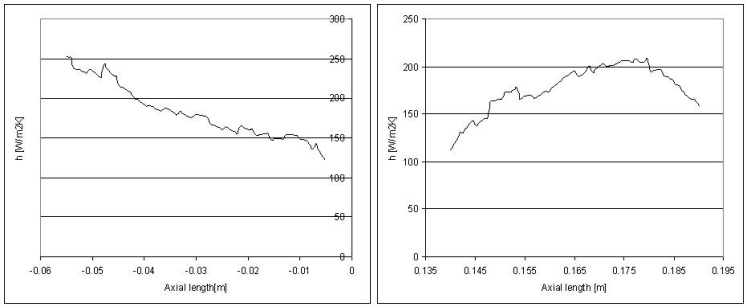

(a) *(b)*

Figure 7.2: The local heat-transfer coefficients of the inlet side (a) and the outlet side (b) of the shaft.

7.3 Heat transfer from the rotor disks

The rotor ends were modelled as rotating disks. The analytical calculations for a rotating disk for the average heat-transfer coefficient $\overline{h_{\mathrm{em}}}$ gave $\overline{h_{\mathrm{em}}} \approx 360 \frac{\mathrm{W}}{\mathrm{m^2K}}$.

The numerical values are presented in Figure 7.3, the inlet side first and the outlet side second. The numerical values were $\overline{h_{\mathrm{nu}}} \approx 310 \frac{\mathrm{W}}{\mathrm{m^2K}}$ and $\overline{h_{\mathrm{nu}}} \approx 175 \frac{\mathrm{W}}{\mathrm{m^2K}}$. The function ends when the corner is reached. From Figure 7.3a one can notice that the heat-transfer coefficient again increases near the corner, exponentially. Near the corner, the fluctuations are enhanced and the flow becomes turbulent which increases exponentially the heat-transfer coefficient.

Figure 7.3b is more interesting. Most of the surface the coefficient is nearly constant. But near the end, there will be a peak. And after that, the coefficient closes to zero. Apparently, the radial velocity component is zero in the cornerpoint. But right next to the corner, the velocity is again able to fluctuate. This causes the peak in the local convection coefficient h.

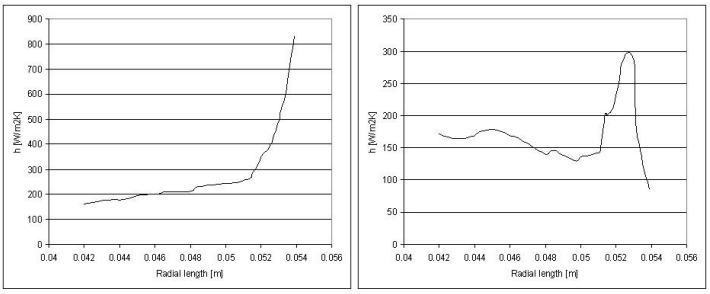

(a) *(b)*

Figure 7.3: The local heat-transfer coefficients of the inlet side (a) and the outlet side (b) of the rotor disk.

7.4 Heat transfer in the end-winding space

7.4.1 The underside area

The lower area of the end-winding can be modeled as a channel again. The dimensions are same as for the shaft. Analytical calculations for the underside heat-transfer coefficient in the end-winding space gave $\overline{h_{\mathrm{em}}} \approx 240 \frac{\mathrm{W}}{\mathrm{m^2K}}$.

The numerical values are $\overline{h_{\mathrm{nu}}} \approx 211 \frac{\mathrm{W}}{\mathrm{m^2K}}$ and $\overline{h_{\mathrm{nu}}} \approx 274 \frac{\mathrm{W}}{\mathrm{m^2K}}$ for the inlet and outlet side of the heat-transfer coefficient, respectively. The empirical value and the numerical values are close to each other. The local heat-transfer coefficient h is presented in Figure 7.4. The fluctuations are due to corners in the end-winding

area but they do not affect too much on the average value. The empirical value gives a good approximation for this surface.

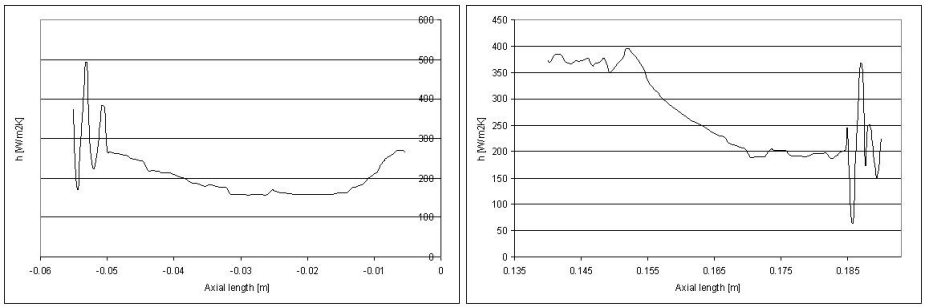

(a) *(b)*

Figure 7.4: The local heat-transfer coefficients from the underside of the end-winding. The inlet side is (a) and the outlet side is (b).

7.4.2 The upside area

The analytical calculations gave the average heat-transfer coefficient value $\overline{h_{\mathrm{em}}} \approx 216 \frac{\mathrm{W}}{\mathrm{m^2K}}$. The numerical values are presented in Figure 7.5. One can see that the heat-transfer coefficient is fluctuating heavily in the region. The velocity around the cylinder surface is fluctuating heavily. The average value for the inlet heat-transfer coefficient is $\overline{h_{\mathrm{nu}}} \approx 530 \frac{\mathrm{W}}{\mathrm{m^2K}}$ and for the outlet coefficient $\overline{h_{\mathrm{nu}}} \approx 356 \frac{\mathrm{W}}{\mathrm{m^2K}}$.

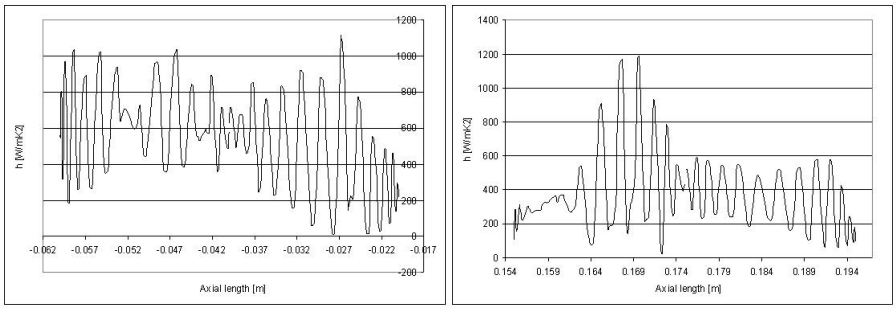

(a) *(b)*

Figure 7.5: The local heat-transfer coefficients from the upside of the end-winding. The inlet side is (a) and the outlet side is (b).

The difference between the inlet and outlet values is due to the difference between the average velocities in the end-winding region. The cooling flow is also warmed up during the cooling procedure which makes the flow hotter when it reaches the

outlet-side end winding. The velocity varies along the surface of the end winding. This causes heavy fluctuations to the heat-transfer coefficient. It is impossible to determine any average velocity for the upside of the end-winding region. For this reason, it is a better option to use the computational fluid dynamics (CFD) for the calculation.

7.5 Heat transfer between the stator core and the frame

The empirical value was $\overline{h_{\mathrm{em}}} \approx 160 \frac{\mathrm{W}}{\mathrm{m^2K}}$. The numerical values are presented in Figure 7.6a and in Figure 7.6b. The numerical value of the average heat-transfer coefficient $\overline{h_{\mathrm{nu}}}$ was $\overline{h_{\mathrm{nu}}} \approx 300 \frac{\mathrm{W}}{\mathrm{m^2K}}$. The coefficient of the stator core resembles that of presented already in the previous chapter of convection. The fluctuation of the heat-transfer coefficients are typical for turbulent boundary layer as already presented in Figure 4.5. Figure 7.6b shows big fluctuations. They are due to the velocity variations on the frame surface.

The analytical equation, Equation 4.33, assumed that $\frac{L}{D} \geq 10$, which means that the length per diameter of the machine should be 10 or more. Actually the ratio of the machine is closer to 2 than to 10. So, the use of this empirical equation should be questioned. The length of the machine is so short that the flow is in the entry region. Two times higher coefficient can be accepted because of the entry region, (Incropera and De Witt, 1990, p.494) This way, the results should be closer to each other.

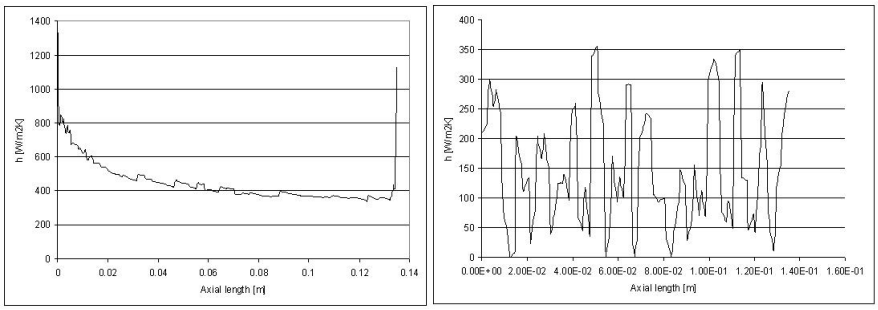

(a) *(b)*

Figure 7.6: The local heat-transfer coefficient h from the stator core and from the stator frame. The average heat-transfer coefficient of these two was $300 \frac{W}{m^2 K}$.

7.6 Heat transfer in the end of the stator core

The empirical value for the average heat-transfer coefficient $\overline{h_{\mathrm{em}}}$ gave $\overline{h_{\mathrm{em}}} \approx 160\frac{\mathrm{W}}{\mathrm{m^2K}}$. The numerical values are presented in Figure 7.7. They resemble those calculated from the rotor disks. The inlet side value was $\overline{h_{\mathrm{nu}}} \approx 420\frac{\mathrm{W}}{\mathrm{m^2}K}$ and the outlet side was $\overline{h_{\mathrm{nu}}} \approx 250\frac{\mathrm{W}}{\mathrm{m^2K}}$. The average of these is $335\frac{\mathrm{W}}{\mathrm{m^2K}}$.

The absolute value of the velocity varies a lot in this region. The heat-transfer coefficient h is defined by the velocity on the surface. The difference between the empirical value and numerical values is big. This is because it is not easy to determine the average velocity on the surface. Another thing is that the empirical model cannot present the fluctuations of the fluid on the surface. These can be modelled only with the computer program.

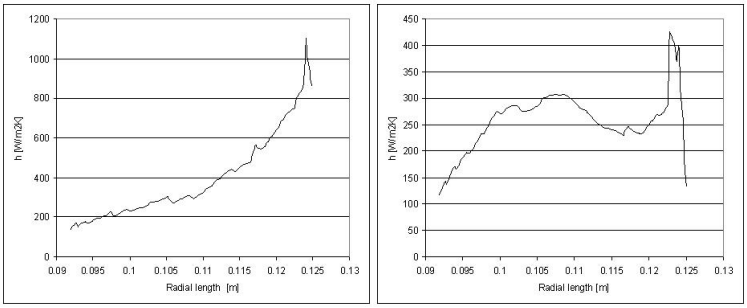

(a) *(b)*

Figure 7.7: The local heat-transfer coefficients of the inlet and outlet sides of the stator yoke end-surfaces.

Chapter 8

Conclusions

Heat-transfer coefficients of convection for a high-speed permanent magnet machine were calculated. They were calculated empirically and numerically with a computer program. Finally, empirical and numerical results were compared to each other. The analytical equations were obtained from the book of Saari (1995).

The empirical and numerical values were close to each other in the air gap. Saari (1995) provides many convection correlations for the Nusselt number in the air gap. The heat transfer in the air gap has been studied quite comprehensively which can be seen from the results. This was the reason why the values were so close to numerical results.

Also the empirical value of the coefficient of convection for the shaft and the underside area of the end-winding can be determined easily. They are simple geometries and there are not too many disturbances affecting the cooling flow in this area. Only the average velocity needs to be determined for these regions.

The other parts of the machine were not so easy to model empirically: The rotor disks, the end of the stator yoke, the upside area of the end winding and the channel between the stator yoke and the stator frame. The problem was that it is not easy to determine the average velocity of the fluid on the surface and the geometry is more complicated.

The computer program shows big fluctuations in the velocity on these surfaces. The fluctuations are produced by the corners in the machine. The airflow behind the end winding is especially turbulent which affects the velocity on the end of the stator yoke surface. These areas can be modelled well enough only numerically with the computer program.

References

Çengel, Yunus A (2002), *Heat transfer: A practical approach. 2^{nd} ed.*, McGraw-Hill Companies, Boston, United States.

Comsol Multiphysics, Heat-transfer Module, User's Guide, Version 3.3 (2006).

Incropera, Frank. De Witt, David P (1990), *Fundamentals of heat and mass transfer 3^{rd} ed.*, McGraw-Hill Companies, New York, United States.

Kays, W. et al. (2005), *Convective Heat and Mass Transfer 4^{th} ed.*, McGraw-Hill, New York, United States.

Kolondzovski, Z (2005), *Pre-Research of high-speed machines*, Helsinki University of Technology, Finland.

Kolondzovski, Z. et al. (2008), Numerical modelling of the coolant flow in a high-speed electrical machine.

Kolondzovski, Z. et al. (2009), 'Multiphysics thermal design of a high-speed permanent-magnet machine', *Elsevier, Applied Thermal Engineering* **29**, 2693–2700.

Lampinen, M.J. et al. (2008), *Lämmonsiirto-oppi*, Laboratory of Applied Thermodynamics (Helsinki University of Technology), Espoo, Finland.

Lähteenmäki, Jussi (2002), *Design and Voltage Supply of High-Speed Induction Machines 1^{st} ed.*, Finnish Academies of Technology, Helsinki, Finland.

Pyrhönen, J. et al. (2008), *Design of Rotating Electrical Machines 1^{st} ed.*, John Wiley & Sons. Ltd, West Sussex, UK.

Pyrhönen, Juha (1991), *The High-Speed Induction Motor: Calculating the Effects of Solid-Rotor Material on Machine Characteristics 1^{st} ed.*, Finnish Academy of Technology, Helsinki, Finland.

Saari, Juha (1995), *Thermal modelling of High-Speed Induction Machines 1^{st} ed.*, Finnish Academy of Technology, Helsinki, Finland.

Saari, Juha (1998), *Thermal Analysis of High-Speed Induction Machines 1^{st} ed.*, Finnish Academy of Technology, Helsinki, Finland.

Shah, R.K. London, A.L (1978), *Laminar flow forced convection in ducts* 1^{st} *ed.*, Academic Press Inc., New York, United States.

Wagner, W (1988), *Wärmeübertragung* 2^{nd} *ed.*, Vogel, Würzburg, Germany.

Zienkiewicz, O.C. et al. (2005), *Finite Element Method for Fluid Dynamics* 6^{th} *ed.*, Elsevier Butterworth-Heinemann, Oxford, UK.

Appendix A: The friction factor for a fully developed flow in a circular tube as a function of the Reynolds number*.

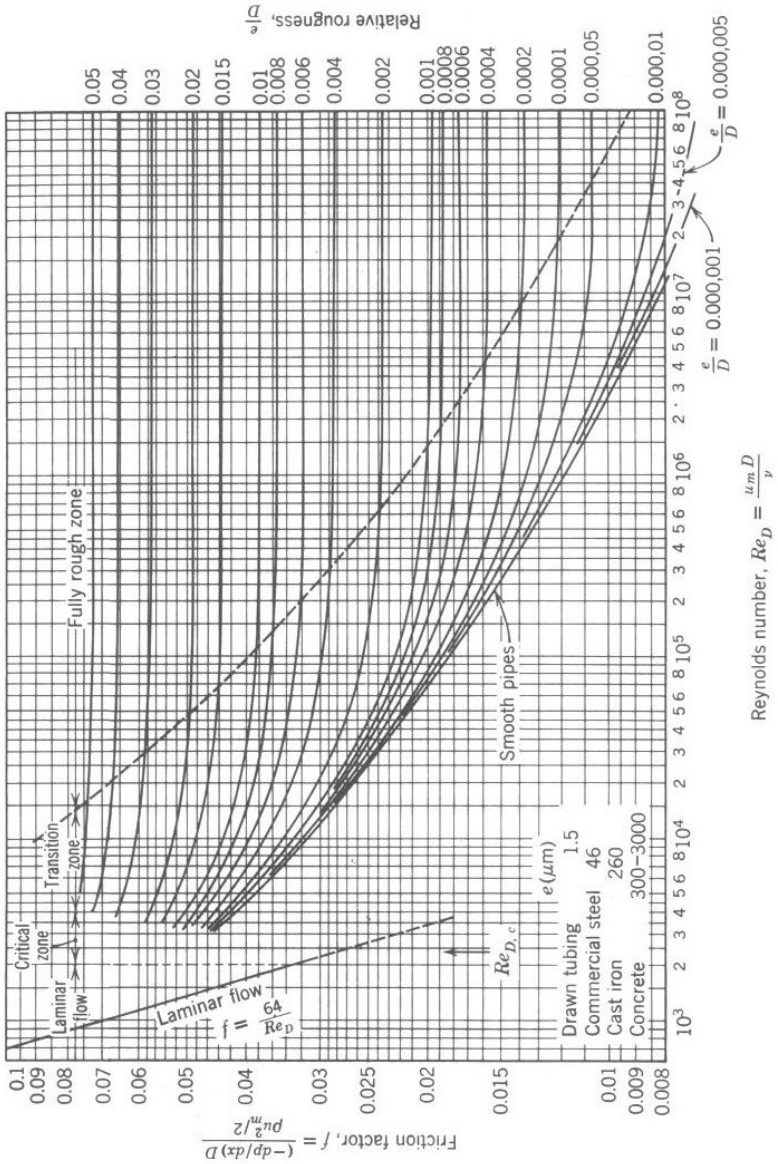

*Incropera and De Witt (1990, p.473)